International Journal of Solids and Structures 48 (2011) 3499–3509

Contents lists available at SciVerse ScienceDirect

International Journal of Solids and Structures

journal homepage: www.elsevier.com/locate/ijsolstr

An elasto-plastic theory of dislocation and disclination fields

C. Fressengeas [a,*], V. Taupin [a], L. Capolungo [b]

[a] Laboratoire d'Etude des Microstructures et de Mécanique des Matériaux, Université Paul Verlaine-Metz/CNRS, Ile du Saulcy, 57045 Metz Cedex, France
[b] G.W. Woodruff School of Mechanical Engineering, Georgia Institute of Technology/CNRS, 57070 Metz Cedex, France

ARTICLE INFO

Article history:
Received 8 April 2011
Received in revised form 25 August 2011
Available online 17 September 2011

Keywords:
Plasticity
Crystal defects
Dislocations
Disclinations
Field dislocation mechanics
Grain boundaries

ABSTRACT

A linear theory of the elasto-plasticity of crystalline solids based on a continuous representation of crystal defects – dislocations and disclinations – is presented. The model accounts for the translational and rotational aspects of lattice incompatibility, respectively associated with the presence of dislocations and disclinations. The defects content relates to the incompatible plastic strain and curvature tensors. The stress state is described by using the conjugate variables to strain and curvature, i.e., the stress and couple-stress tensors. Defect motion is described by two transport equations. A dynamic interplay between dislocations and disclinations results from a disclination-induced source term in the transport of dislocations. Thermodynamic guidance provides the driving forces conjugate to dislocation and disclination velocity in a continuous context, as well as admissible constitutive relations for the latter. When dislocation and disclination velocity vanish, the model reduces to deWit's elasto-static theory of crystal defects. It also reduces to Acharya's linear elasto-plastic theory for dislocation fields when the disclination density is ignored. The theory is intended for use in instances where rotational defects matter, such as grain boundaries. To illustrate its applicability, a finite high-angle tilt boundary is modeled using a disclination dipole and its behavior under tensile loading normal to the boundary is shown.

1. Introduction

With motivations deriving from Weingarten's theorem (Weingarten, 1901), disclinations and dislocations were simultaneously introduced by Volterra, as early as the turn of the last century (Volterra, 1907). Dislocations are the crystal defects arising from translational lattice incompatibility, as measured by the Burgers vector, whereas disclinations are defects originating in the rotational incompatibility of the crystal lattice, as characterized by the Frank's vector (deWit, 1970). Disclinations have long been considered as secondary topics in the field theory of crystal defects, due to the very large level of elastic energy they involve, as compared with dislocations, which precludes their occurrence as isolated crystalline objects (Friedel, 1964). However self-screened configurations, such as disclination dipoles, involve relatively small elastic energy levels (Romanov and Vladimirov, 1992; Romanov and Kolesnikova, 2009). Hence, they may enter the description of the lattice structure when a single-valued elastic rotation field does not exist. Grain boundaries are such instances and, as rotational defects, disclinations may prove useful in their modeling (Li, 1972). A series of examples in relation with this idea was given in a recent review paper (Kleman and Friedel, 2008) (also concerned with liquid crystals), namely: high-angle boundaries, grain boundary ledges, grain boundaries as sources and sinks for dislocations, grain rotation in polynanocrystals. . .Yet, as suggested above, dislocation-based models have been preferentially used for that purpose over the last decades. Employing the Frank-Bilby surface-dislocation concept (Frank, 1950; Bilby, 1955), they have become widely accepted for low angle boundaries. Well-known examples are the tilt and twist boundaries. However, the dislocation-based models suffer from several limitations. Considering infinite dislocation walls makes it difficult to model the three-dimensional network of grain boundaries in a polycrystal. Accounting for high-angle boundaries requires packing dislocations so tightly along the interface that their cores must overlap. Perhaps more to the point, boundaries are seen as infinitely thin planes. Yet, grain boundaries feature spatial patterns referred to as structural units spreading over a finite width area (Sutton and Vitek, 1983). Disclination-based models remove these limitations. They may be used to model finite high-angle boundaries, and to account for their fine structure (Li, 1972; Shih and Li, 1975; Gertsman et al., 1989; Hurtado et al., 1995).

In the present paper, the aim is to present a field defect (dislocation and disclination) theory for crystal plasticity accounting for both the translational and rotational aspects of lattice incompatibility. To focus on the relevant physical ideas and avoid the complications arising from geometric nonlinearity, we limit the presentation

* Corresponding author.
E-mail address: claude.fressengeas@univ-metz.fr (C. Fressengeas).

0020-7683/$ - see front matter © 2011 Elsevier Ltd. All rights reserved.
doi:10.1016/j.ijsolstr.2011.09.002

to infinitesimal transformations, leaving the differential geometry developments inherent to finite transformations for future work. By a field theory, we mean a theory of continuously distributed crystal defects using the mathematical tools of the theory of partial differential equations and boundary problems solving. As such, we capitalize on the earlier elasto-static theories of dislocation fields (Kröner et al., 1980; Kröner, 1958) and of crystal defects (dislocations and disclinations) (deWit, 1970). Both theories are strongly connected: the latter reduces to the former when the disclination density vanishes. We also benefit from the more recent mechanical theory of dislocation fields (Acharya, 2001), which deals with crystal plasticity. In this theory, the material displacements as well as the density and motion of dislocations can be derived uniquely from initial and boundary conditions, provided constitutive information for elasticity and the dislocation velocity is supplied (Acharya, 2003). When the dislocation velocity vanishes, the field dislocation mechanics theory (Acharya, 2001) reduces to the elasto-static theory of dislocations (Kröner et al., 1980; Kröner, 1958). As we shall demonstrate below, the present framework reduces to field dislocation mechanics when the disclination density is ignored, and to the elasto-static crystal theory of defects (deWit, 1970) when the velocities of dislocations and disclinations vanish. A previous attempt at a theory of plasticity accounting for both the translational and rotational aspects of lattice incompatibility was that of Kossecka and deWit (1977). The theory offered kinematic guidelines, but did not provide driving forces and was not applied towards the solution of a realistic boundary value problem. Our goal in putting forward this model is to deal with situations where the dynamic interplay between dislocations and disclinations is essential to the understanding of the defect structure. Such a situation is described in a companion paper (Upadhyay et al., in press), where a disclination-based framework is used to quantify the effect of rotational incompatibility on the elastic energy of symmetric tilt boundaries and triple junctions in face centered cubic materials. The analysis strongly suggests that a complete understanding of the stability of triple junctions cannot be obtained through energy minimization, and is only achievable through a dynamic mechanical model of linear crystal defects. We shall illustrate this point of view by investigating the nucleation and motion under applied loading of disclination dipoles, perhaps the simplest possible case-study, but also the one where the structure of the governing equations of the model is the more self-evident.

The paper is organized as follows. In Section 2, notation conventions are settled. For the sake of completeness, we provide a brief review of the incompatible elastic defect theory (deWit, 1970) in Section 3. Static coupling between dislocations and disclinations is included at this level, through the continuity condition for dislocation densities and the Cosserat equilibrium equation for couple-stresses (Cosserat and Cosserat, 1909). Section 4 is devoted to the transport properties of dislocations and disclinations. Dynamic coupling occurs at this stage, since disclination mobility provides for a source term in the transport equation for dislocations. In Section 5, guidance of the Clausius–Duhem inequality is sought to define the driving forces associated with the dislocation and disclination velocities, as well as appropriate constitutive relations between these forces and velocities. Section 6 deals with the algorithms used for the solution of the governing equations. A plane "edge–wedge" model is detailed in Section 7, and used in Section 8 to investigate the structure and mobility of disclination dipoles. Concluding remarks follow.

2. Notations

A bold symbol denotes a tensor. When there may be ambiguity, an arrow is superposed to represent a vector: $\vec{\mathbf{V}}$. The symmetric part of tensor $\mathbf{A}$ is denoted $\{\mathbf{A}\}$. The symbol $\mathbf{A}.\mathbf{B}$ represents multiplication of the tensors $\mathbf{A}$ and $\mathbf{B}$, and $\mathbf{A}\otimes\mathbf{B}$ their tensorial product. A: represents the trace inner product of the two second order tensors $\mathbf{A}:\mathbf{B}=A_{ij}B_{ij}$, in rectangular Cartesian components, or the product of a higher order tensor with a second order tensor, e.g., $\mathbf{A}:\mathbf{B}=A_{ijkl}B_{kl}$. The cross product of a second-order tensor $\mathbf{A}$ and a vector $\mathbf{V}$, the **div** and **curl** operations for second-order tensors are defined row by row, in analogy with the vectorial case. For any base vector $\mathbf{e}_i$ of the reference frame:

$$(\mathbf{A}\times\mathbf{V})^t.\mathbf{e}_i=(\mathbf{A}^t.\mathbf{e}_i)\times\mathbf{V}, \tag{1}$$

$$(\mathbf{div}\ \mathbf{A})^t.\mathbf{e}_i=\mathbf{div}(\mathbf{A}^t.\mathbf{e}_i), \tag{2}$$

$$(\mathbf{curl}\ \mathbf{A})^t.\mathbf{e}_i=\mathbf{curl}(\mathbf{A}^t.\mathbf{e}_i). \tag{3}$$

In rectangular Cartesian components:

$$(\mathbf{A}\times\mathbf{V})_{ij}=e_{jkl}A_{ik}V_l, \tag{4}$$

$$(\mathbf{div}\ \mathbf{A})_i=A_{ij,j}, \tag{5}$$

$$(\mathbf{curl}\ \mathbf{A})_{ij}=e_{jkl}A_{il,k}. \tag{6}$$

where e_{jkl} is a component of the third-order alternating Levi–Civita tensor $\mathbf{X}$. A vector $\overrightarrow{\mathbf{A}}$ is associated with tensor $\mathbf{A}$ by using its trace inner product with tensor $\mathbf{X}$:

$$(\overrightarrow{\mathbf{A}})_k=-\frac{1}{2}(\mathbf{A}:\mathbf{X})_k=-\frac{1}{2}e_{ijk}A_{ij}. \tag{7}$$

In the component representation, the spatial derivative with respect to a Cartesian coordinate is indicated by a comma followed by the component index. A superposed dot represents a material time derivative.

3. Review of the incompatible elasto-static defect theory

In the present framework, it is assumed that the displacement vector $\mathbf{u}$ can be defined continuously at any point of a simply-connected body undergoing elasto-plastic deformation. Hence, it is required that the displacement field represent a consistent shape change, possibly defined between atoms, below interatomic distance. Therefore, the total distortion tensor is defined as the gradient of the displacement $\mathbf{U}=\mathbf{grad}\ \mathbf{u}$. As such, it is curl-free:

$$\mathbf{curl}\ \mathbf{U}=0. \tag{8}$$

This equation is a necessary condition for the integrability of the displacement $\mathbf{u}$ and a compatibility condition for the distortion $\mathbf{U}$. In the elasto-plastic theory of dislocations, such is not the case in general for its plastic, $\mathbf{U_p}$, and elastic, $\mathbf{U_e}$, components. Then, an incompatible part, $\mathbf{U_p^\perp}$, which is not curl-free, exists in the plastic distortion tensor, due to the presence of dislocations, and an opposite incompatible elastic distortion of the lattice, $\mathbf{U_e^\perp}$, arises to maintain lattice continuity. Curl-free compatible components, $\mathbf{U_e^\parallel}$ and $\mathbf{U_p^\parallel}$, may also exist to satisfy the balance of equilibrium and boundary conditions, and the following relations are therefore satisfied:

$$\mathbf{U}=\mathbf{U_e}+\mathbf{U_p}, \tag{9}$$

$$\mathbf{U_e}=\mathbf{U_e^\perp}+\mathbf{U_e^\parallel}, \tag{10}$$

$$\mathbf{U_p}=\mathbf{U_p^\perp}+\mathbf{U_p^\parallel}, \tag{11}$$

$$0=\mathbf{U_e^\perp}+\mathbf{U_p^\perp}, \tag{12}$$

$$\mathbf{curl}\ \mathbf{U_e^\perp}=-\mathbf{curl}\ \mathbf{U_p^\perp}=\boldsymbol{\alpha}\neq 0. \tag{13}$$

Composing Eqs. (9)–(11) shows that Eq. (12) is needed to ensure that the compatibility condition (8) is satisfied. On the one hand, the incompatibility Eq. (13) define the incompatible plastic distortion $\mathbf{U_p^\perp}$ associated with the presence of Nye's dislocation density tensor $\boldsymbol{\alpha}$, and on the other hand they provide the incompatible elas-

tic distortion $\mathbf{U}_\mathbf{e}^{\perp}$ offsetting the latter to ensure the continuity of matter.[1] Since $\mathbf{U}_\mathbf{e}^{\parallel}$ and $\mathbf{U}_\mathbf{p}^{\parallel}$ are curl-free, Eq. (13) is still true when $\mathbf{U}_e^{\perp}$ and $\mathbf{U}_\mathbf{p}^{\perp}$ are respectively replaced with $\mathbf{U_e}$ and $\mathbf{U_p}$:

$$\mathbf{curl}\ \mathbf{U_e} = -\mathbf{curl}\ \mathbf{U_p} = \boldsymbol{\alpha}. \tag{14}$$

Therefore, to ensure that the incompatible part $\mathbf{U}_\mathbf{p}^{\perp}$ vanishes identically throughout the body when $\boldsymbol{\alpha} = 0$, Eq. (13) must be augmented with the side conditions $\mathbf{div}\ \mathbf{U}_\mathbf{p}^{\perp} = \mathbf{0}$ and $\mathbf{U}_\mathbf{p}^{\perp}.\mathbf{n} = \mathbf{0}$ on the boundary with unit normal $\mathbf{n}$. Further, the continuity condition:

$$\mathbf{div}\boldsymbol{\alpha} = 0, \tag{15}$$

follows directly from Eqs. (13) and (14).

Defining the strain tensor $\boldsymbol{\epsilon}$ as the symmetric part of the distortion $\mathbf{U}$, the rotation tensor $\boldsymbol{\omega}$ as its skew-symmetric part and the associated rotation vector $\vec{\omega}$ as:

$$\vec{\omega} = -\frac{1}{2}\boldsymbol{\omega} : \mathbf{X}. \tag{16}$$

Eq. (8) becomes:

$$\mathbf{curl}\ \boldsymbol{\epsilon} + div(\vec{\omega})\mathbf{I} - \mathbf{grad}^{\mathbf{t}}\vec{\omega} = 0, \tag{17}$$

where $\mathbf{I}$ is the identity tensor. Transposing, then taking the **curl** of Eq. (17) leads to:

$$\mathbf{curl}\ \mathbf{curl}^{\mathbf{t}}\boldsymbol{\epsilon} = 0. \tag{18}$$

This relation is the classical Saint–Venant compatibility condition for the strain $\boldsymbol{\epsilon}$. It is a necessary condition for the integrability of the displacement $\mathbf{u}$. The trace of Eq. (17) similarly yields a compatibility condition for the rotation vector in the form:

$$div(\vec{\omega}) = 0. \tag{19}$$

Applying the same curl-trace procedure to the elastic restriction of Eq. (14), we obtain from the curl operation, with self-evident notations, an equation parallel to Eq. (17):

$$\mathbf{curl}\ \boldsymbol{\epsilon}_e + div(\vec{\omega}_e)\mathbf{I} - \mathbf{grad}^{\mathbf{t}}\vec{\omega}_e = \boldsymbol{\alpha}, \tag{20}$$

and a similar equation for the plastic restriction of Eq. (14):

$$\mathbf{curl}\ \boldsymbol{\epsilon}_p + div(\vec{\omega}_p)\mathbf{I} - \mathbf{grad}^{\mathbf{t}}\vec{\omega}_p = -\boldsymbol{\alpha}. \tag{21}$$

As elastic and plastic rigid body rotations, $(\vec{\omega}_e, \vec{\omega}_p)$ are integrable quantities. From the trace operation, we find an equation parallel to Eq. (19):

$$div(\vec{\omega}_e) = -div(\vec{\omega}_p) = \frac{1}{2}tr(\boldsymbol{\alpha}). \tag{22}$$

Motivated by the Saint–Venant compatibility condition (18), we transpose Eqs. (20) and (21) and further rearrange with the help of Eq. (22), to obtain:

$$\mathbf{grad}\ \vec{\omega}_e = \mathbf{curl}^{\mathbf{t}}\boldsymbol{\epsilon}_e + \mathbf{K}, \tag{23}$$

$$\mathbf{grad}\ \vec{\omega}_p = \mathbf{curl}^{\mathbf{t}}\boldsymbol{\epsilon}_p - \mathbf{K}, \tag{24}$$

$$\mathbf{K} = \frac{1}{2}tr(\boldsymbol{\alpha})\mathbf{I} - \boldsymbol{\alpha}^t. \tag{25}$$

At this point, we can define the elastic, $\boldsymbol{\kappa}_e$, and plastic, $\boldsymbol{\kappa}_p$, curvature tensors as:

$$\boldsymbol{\kappa}_e = \mathbf{grad}\ \vec{\omega}_e, \tag{26}$$

$$\boldsymbol{\kappa}_p = \mathbf{grad}\ \vec{\omega}_p, \tag{27}$$

$$\mathbf{grad}\ \vec{\omega} = \boldsymbol{\kappa}_e + \boldsymbol{\kappa}_p, \tag{28}$$

and take the **curl** of Eqs. (23) and (24), to find:

$$\mathbf{curl}\boldsymbol{\kappa}_e = \mathbf{curl}\ \mathbf{curl}^{\mathbf{t}}\boldsymbol{\epsilon}_e + \mathbf{curl}\ \mathbf{K} = 0, \tag{29}$$

$$\mathbf{curl}\boldsymbol{\kappa}_p = \mathbf{curl}\ \mathbf{curl}^{\mathbf{t}}\boldsymbol{\epsilon}_p - \mathbf{curl}\ \mathbf{K} = 0. \tag{30}$$

Hence, in the elasto-plastic theory of dislocations, the elastic and plastic curvatures $(\boldsymbol{\kappa}_e, \boldsymbol{\kappa}_p)$ are curl-free and, as mentioned above, the rotation vectors $(\vec{\omega}_e, \vec{\omega}_p)$ are integrable quantities. $\mathbf{K}$ is Nye's curvature tensor (Nye, 1953), sometimes used to estimate the curvature tensors $(\boldsymbol{\kappa}_e, \boldsymbol{\kappa}_p)$ by neglecting the contributions of the incompatible elastic and plastic strains. $(\boldsymbol{\kappa}_e, \boldsymbol{\kappa}_p)$ are also known as the elastic and plastic bend-twist tensors, respectively.

If $(\boldsymbol{\kappa}_e, \boldsymbol{\kappa}_p)$ are not supposed to be curl-free anymore, i.e., if the possibility of a rotational incompatibility is acknowledged, then the rigid body rotations $(\vec{\omega}_e, \vec{\omega}_p)$ do not exist, and a non-zero tensor $\boldsymbol{\theta}$ such that

$$\boldsymbol{\theta} = -\mathbf{curl}\ \boldsymbol{\kappa}_p = \mathbf{curl}\ \boldsymbol{\kappa}_e, \tag{31}$$

can be defined. $\boldsymbol{\theta}$ is the disclination density tensor, and Eq. (31) is part of the theory of crystal defects. It replaces Eqs. (29) and (30), which pertain to the theory of dislocations. On the one hand, Eq. (31) means that an incompatible plastic curvature, $\boldsymbol{\kappa}_p^{\perp}$, is associated with the presence of the disclination density $\boldsymbol{\theta}$ and, on the other hand, that the incompatible elastic curvature, $\boldsymbol{\kappa}_e^{\perp}$ is needed to ensure the continuity of matter in the presence of this density. As already discussed for the translational incompatibility, to ensure that the incompatible parts $\left(\boldsymbol{\kappa}_e^{\perp}, \boldsymbol{\kappa}_p^{\perp}\right)$ vanish identically throughout the body when $\boldsymbol{\theta} = 0$, Eq. (31) must be replaced with:

$$\boldsymbol{\theta} = -\mathbf{curl}\ \boldsymbol{\kappa}_p^{\perp} = \mathbf{curl}\ \boldsymbol{\kappa}_e^{\perp}, \tag{32}$$

augmented with the side conditions $\mathbf{div}\,\boldsymbol{\kappa}_e^{\perp} = \mathbf{div}\,\boldsymbol{\kappa}_p^{\perp} = 0$ and $\boldsymbol{\kappa}_e^{\perp}.\mathbf{n} = \boldsymbol{\kappa}_p^{\perp}.\mathbf{n} = 0$ on the boundary with unit normal $\mathbf{n}$. These conditions ensure uniqueness of the solution. The continuity condition for disclinations:

$$\mathbf{div}\ \boldsymbol{\theta} = 0, \tag{33}$$

follows directly from Eqs. (31) and (32). Since the rigid body rotations $(\vec{\omega}_e, \vec{\omega}_p)$ do not exist in the theory of crystal defects, the corresponding elastic and plastic distortion tensors $\mathbf{U}_e$ and $\mathbf{U}_p$ are also undefined. Substituting the elastic and plastic curvatures $(\boldsymbol{\kappa}_e, \boldsymbol{\kappa}_p)$, which now include an incompatible part, for $(\mathbf{grad}\ \vec{\omega}_e, \mathbf{grad}\ \vec{\omega}_p)$ in Eqs. (20) and (21), leads to the modified equations:

$$\mathbf{curl}\ \boldsymbol{\epsilon}_e = +\boldsymbol{\alpha} + \boldsymbol{\kappa}_e^t - tr(\boldsymbol{\kappa}_e)\mathbf{I}, \tag{34}$$

$$\mathbf{curl}\ \boldsymbol{\epsilon}_p = -\boldsymbol{\alpha} + \boldsymbol{\kappa}_p^t - tr(\boldsymbol{\kappa}_p)\mathbf{I}. \tag{35}$$

Eq. (35) defines the incompatible plastic strain associated with the dislocation density tensor $\boldsymbol{\alpha}$ in the concurrent presence of plastic curvature, while Eq. (34) specifies the incompatible elastic strain needed to ensure the continuity of matter in the presence of dislocations and disclinations. Eq. (34) may be utilized to estimate Nye's tensor from high resolution EBSD experiments. It also suggests that the true state quantities to be used in specifying the free energy of the body are the elastic strain $\boldsymbol{\epsilon}_e$ and elastic curvature $\boldsymbol{\kappa}_e$ tensors (see below Eq. (47)). If the incompatibility tensor $\boldsymbol{\eta}$ is defined as:

$$\boldsymbol{\eta} = \mathbf{curl}\ \mathbf{curl}^{\mathbf{t}}\ \boldsymbol{\epsilon}_p, \tag{36}$$

it is seen from Eqs. (30) and (31) that:

$$\boldsymbol{\eta} = \mathbf{curl}\ \mathbf{K} - \boldsymbol{\theta}. \tag{37}$$

When dislocations and disclinations are absent, we find: $\boldsymbol{\eta} = 0$, which shows that $\boldsymbol{\eta}$ is indeed a measure of incompatibility. When

[1] By virtue of Stoke's theorem: $\int_C \mathbf{U}.\mathbf{dl} = \int_S \mathbf{curl}\mathbf{U}.\mathbf{n}dS$ on a closed curve C surrounding surface S of normal $\mathbf{n}$. In compatible theory, the distortion tensor $\mathbf{U}$ is a gradient and its circulation along curve C is zero on the left hand side. Thus, from the right hand side, the compatibility condition (8) is satisfied with sufficient continuity. In the presence of a net content of dislocations threading S, a discontinuity in the elastic displacement arises, and the closure defect of circuit C : $\mathbf{b} = \int_C \mathbf{U_e}.\mathbf{dl}$ is non zero. $\mathbf{b}$ is referred to as the Burgers vector of the dislocations threading S. It characterizes the incompatibility in the elastic displacement along circuit C. The left Eqs. (13, 14) are now satisfied, and the net dislocation content is also characterized in a continuous manner by Nye's tensor $\boldsymbol{\alpha}$.

only dislocations are present, $\boldsymbol{\eta} = \mathbf{curl}\ \mathbf{K}$, while Eq. (37) describes how dislocations and disclinations respectively participate to the overall incompatibility. The continuity condition (15) for dislocations is also modified in the theory of crystal defects. Taking the divergence of Eq. (34) and defining the twist-disclination vector $\vec{\boldsymbol{\Theta}}$ as:

$$\vec{\boldsymbol{\Theta}} = -\frac{1}{2}\boldsymbol{\theta} : \mathbf{X}, \tag{38}$$

it is found that:

$$\mathbf{div}\ \boldsymbol{\alpha} + 2\vec{\boldsymbol{\Theta}} = 0. \tag{39}$$

This continuity equation implies the existence of geometric interactions between twist- disclinations ($i \neq j$) and dislocations. Of course, when the disclination density vanishes, Eqs. 34, 35, 39 reduce to Eqs. (14), (15), and the elastic theory of crystal defects reduces to the theory of dislocations.

In the theory of crystal defects, the Frank's and Burgers vectors for a close circuit C bounding a surface S are defined as (deWit, 1970):

$$\boldsymbol{\Omega} = \int_C \boldsymbol{\kappa}_e.\mathbf{dr}, \tag{40}$$

$$\mathbf{b} = \int_C (\boldsymbol{\epsilon}_e - \boldsymbol{\kappa}_e \times \mathbf{r}).\mathbf{dr}. \tag{41}$$

They can be related to the dislocation and disclination density tensors $\boldsymbol{\alpha}$ and $\boldsymbol{\theta}$ by applying Stoke's theorem to the surface S (deWit, 1970):

$$\boldsymbol{\Omega} = \int_S \boldsymbol{\theta}.\mathbf{n}dS, \tag{42}$$

$$\mathbf{b} = \int_S (\boldsymbol{\alpha} - \boldsymbol{\theta} \times \mathbf{r}).\mathbf{n}dS. \tag{43}$$

From Eq. (42), it is seen that, for a unit surface of normal $\mathbf{n}$, the disclination density tensor can alternatively be written:

$$\boldsymbol{\theta} = \boldsymbol{\Omega} \otimes \mathbf{n}. \tag{44}$$

The material displacement $\mathbf{u}$ and rotation vector $\vec{\boldsymbol{\omega}}$ are independent kinematic variables, which can be integrated from the knowledge of $\boldsymbol{\epsilon}_e$ and $\boldsymbol{\kappa}_e$. The conjugate variables to the latter are the stress and couple-stress tensors, and the equilibrium equations are, in the absence of body forces:

$$\mathbf{div}\ \mathbf{T} = 0, \tag{45}$$

$$\mathbf{div}\ \mathbf{M} + 2\vec{\mathbf{T}} = 0. \tag{46}$$

Here $\mathbf{T}$ is the (generally non-symmetric) stress tensor, $\vec{\mathbf{T}}$ the stress vector defined as $\vec{\mathbf{T}} = -1/2\mathbf{T} : \mathbf{X}$, and $\mathbf{M}$ is the couple-stress tensor. In principle, boundary conditions on the stress and couple-stress are therefore needed. In this sense, the theory of crystal defects defines a Cosserat continuum. A specific free energy density function is introduced as follows:

$$\psi = \psi(\boldsymbol{\epsilon}_e, \boldsymbol{\kappa}_e). \tag{47}$$

As already suggested, ψ contains contributions to the stored energy from the elastic strain $\boldsymbol{\epsilon}_e$ and curvature $\boldsymbol{\kappa}_e$ arising from the presence of crystal defects and the application of loads. At nanoscale (for instance in dislocation core problems), the body is seen as a continuum containing material points between atoms, capable of transmitting stresses and couple-stresses at this scale, and ψ presents nonlinear and non-convex properties to respect the periodicity of the lattice. At larger scales, lattice fluctuations may be overlooked and ψ may be taken as a convex function of elastic strain and curvature. Differentiating Eq. (47), we obtain the following identification of the stress and couple-stress tensors with the partial derivatives of the free energy:

$$\dot{\psi} = \frac{\partial \psi}{\partial \boldsymbol{\epsilon}_e} : \dot{\boldsymbol{\epsilon}}_e + \frac{\partial \psi}{\partial \boldsymbol{\kappa}_e} : \dot{\boldsymbol{\kappa}}_e = \mathbf{T} : \dot{\boldsymbol{\epsilon}}_e + \mathbf{M} : \dot{\boldsymbol{\kappa}}_e. \tag{48}$$

The elastic constitutive relations for $\mathbf{T}$ and $\mathbf{M}$ are consistently chosen in the form suggested in deWit (1970):

$$\mathbf{T} = \mathbf{C} : \boldsymbol{\epsilon}_e + \mathbf{D} : \boldsymbol{\kappa}_e, \tag{49}$$

$$\mathbf{M} = \mathbf{A} : \boldsymbol{\kappa}_e + \mathbf{B} : \boldsymbol{\epsilon}_e. \tag{50}$$

Here $\mathbf{A}$, $\mathbf{B}$, $\mathbf{C}$ and $\mathbf{D}$ are tensors of elastic constants. While the C_{ijkl} and A_{ijkl} constants have dimension of a stress and a stress times a squared length respectively, B_{ijkl} and D_{ijkl} have dimension of a stress multiplied by a length. Hence, the relations (49) and (50) involve characteristic lengths and have nonlocal character. The tensor $\mathbf{D}$ induces stresses due to the inhomogeneity in rotation over some (short) length scale, while the tensor $\mathbf{B}$ gives rise to couple stresses from inhomogeneity in strain over some other (short) length scale. Further detail will be provided in Section 7 in a specific problem.

4. Transport of dislocations and disclinations

Consider a material surface S bounded by a closed curve C. Let $\mathbf{f}$ be the disclination flux field used to measure the rate of inflow into S of disclination lines, carrying along with them their corresponding Frank vectors $\boldsymbol{\Omega}$, through a line element $\mathbf{dx}$ of curve C. Let $\mathbf{V}_\theta$ be the velocity of the disclinations with respect to the lattice, and $\mathbf{l}$ the unit vector along the disclination lines. Then the disclination tensor is: $\boldsymbol{\theta} = \boldsymbol{\Omega} \otimes \mathbf{l}$. In the absence of any disclination source term, the conservation of the Frank's vector content demands that the rate of change of the Frank's vector of all disclination lines threading S be equal to the total disclination flux across curve C:

$$\frac{d}{dt}\int_S \boldsymbol{\theta}.\mathbf{n}dS = \int_C \mathbf{f}.\mathbf{dx}. \tag{51}$$

For small transformations, the point-wise statement corresponding to (51) is:

$$\dot{\boldsymbol{\theta}} = \mathbf{curl}\ \mathbf{f} \tag{52}$$

where $\dot{\boldsymbol{\theta}}$ represents the time derivative of the disclination density tensor. The rate of inflow of Frank vectors across the surface $\mathbf{dS} = \mathbf{l} \times \mathbf{dx}$ is:

$$\mathbf{f}.\mathbf{dx} = \boldsymbol{\Omega}(\mathbf{V}_\theta.\mathbf{dS}) \tag{53}$$

Some manipulations then lead to:

$$\mathbf{f} = -\boldsymbol{\Omega} \otimes \mathbf{l} \times \mathbf{V}_\theta = -\boldsymbol{\theta} \times \mathbf{V}_\theta. \tag{54}$$

Consequently, the local statement of balance (52) becomes:

$$\dot{\boldsymbol{\theta}} = -\mathbf{curl}(\boldsymbol{\theta} \times \mathbf{V}_\theta). \tag{55}$$

Comparison with Eq. (31) shows, after a derivation of the latter with respect to time, that the cross product in (55) can be identified with the plastic curvature rate tensor:

$$\dot{\boldsymbol{\kappa}}_p = \boldsymbol{\theta} \times \mathbf{V}_\theta. \tag{56}$$

Eq. (55) is a transport law for the disclination density tensor $\boldsymbol{\theta}$. It can be understood as an evolution law for $\boldsymbol{\theta}$, provided the disclination velocity $\mathbf{V}_\theta$ is known as a function of the stress state from constitutive statements. Its meaning is that, through the curl term, the incompatible part of the plastic curvature rate, $\dot{\boldsymbol{\kappa}}_p^{\perp}$, incrementally feeds the disclination density. As we shall discuss below, the compatible part $\dot{\boldsymbol{\kappa}}_p^{\parallel}$ increments the history-dependent compatible plastic curvature produced by the motion of dislocations and disclinations.

In the theory of dislocations, the dislocation density tensor $\boldsymbol{\alpha}$ satisfies a transport equation similar to Eq. (55), in the absence of a source term (Acharya, 2001; Mura, 1963):

$$\dot{\boldsymbol{\alpha}} = -\mathbf{curl}\ (\boldsymbol{\alpha} \times \mathbf{V}_\alpha) = -\mathbf{curl}\ \dot{\mathbf{U}}_p. \tag{57}$$

Here, $\mathbf{V}_\alpha$ denotes the dislocation velocity. However, the plastic distortion rate $\dot{\mathbf{U}}_p$ is undefined in the theory of crystal defects, where only its symmetric part $\dot{\boldsymbol{\epsilon}}_p$ can be prescribed:

$$\dot{\boldsymbol{\epsilon}}_p = \frac{1}{2}\left(\boldsymbol{\alpha} \times \mathbf{V}_\alpha + (\boldsymbol{\alpha} \times \mathbf{V}_\alpha)^t\right). \tag{58}$$

The transport equation of the theory of dislocations has therefore to be modified. For small transformations, it is readily obtained from a time derivative of Eq. (35):

$$\dot{\boldsymbol{\alpha}} = -\mathbf{curl}\ \dot{\boldsymbol{\epsilon}}_p + \dot{\boldsymbol{\kappa}}_p^t - tr(\dot{\boldsymbol{\kappa}}_p)\mathbf{I} = -\mathbf{curl}\ \dot{\boldsymbol{\epsilon}}_p + \mathbf{s}_\theta. \tag{59}$$

An outstanding consequence of Eq. (59) is that dislocations are nucleated not only because the plastic strain rate has an incompatible part, $\dot{\boldsymbol{\epsilon}}_p^\perp$, but also because a source term, $\mathbf{s}_\theta = \dot{\boldsymbol{\kappa}}_p^t - tr(\dot{\boldsymbol{\kappa}}_p)\mathbf{I}$, involving the mobility of the disclinations is existing. Thus, a wake of dislocations (nucleated or absorbed) is accompanying the motion of disclinations. In contrast with the dislocations arising from lattice incompatibility (the curl term in Eq. (59)), this wake of dislocations may be seen as systematically contributing to the relaxation of internal stresses in the neighborhood of disclinations (Romanov and Vladimirov, 1992; Kleman and Friedel, 2008). When the dislocation and disclination velocities are known from the stress state through constitutive relations, Eq. (59) can be used as an evolution equation for the dislocation densities. Of course, the compatible part of the plastic strain rate, $\dot{\boldsymbol{\epsilon}}_p^\parallel$, increments the compatible strain produced by the motion of dislocations through the lattice. Note that, like the transport equation for disclinations (55), Eq. (59) has propagative character. Fundamental implications on the mathematical nature of the boundary value problem derive from this property, which has also a strong impact on the algorithms devoted to its solution (see for example Varadhan et al., 2006).

5. Constitutive relations for the dislocation and disclination velocities

In Eqs. (55), (59) the dislocation and disclination velocities $(\mathbf{V}_\alpha, \mathbf{V}_\theta)$ need to be constitutively specified. In doing so below, we seek guidance in a procedure originally introduced in (Coleman and Gurtin, 1967). We first look for the driving forces associated with the dislocation and disclination velocities. The mechanical dissipation in the body D is defined as the difference between the power of the applied forces and the rate of change of the stored energy, i.e.

$$\begin{aligned} D &= \int_{\partial D} (\mathbf{v}.\mathbf{T} + \dot{\vec{\boldsymbol{\omega}}}.\mathbf{M}).\mathbf{n} dS - \int_D \dot{\psi} dv \\ &= \int_{\partial D} (v_i T_{ij} + \dot{\omega}_i M_{ij}) n_j dS - \int_D \dot{\psi} dv. \end{aligned} \tag{60}$$

Here, $\mathbf{v}$ is the material velocity, and volumetric forces and couples are ignored for the sake of simplicity. Using the divergence theorem and the Cosserat equilibrium Eqs. (45) and (46), we can also write in component form:

$$D = \int_D [(v_i T_{ij} + \dot{\omega}_i M_{ij})_{,j} - v_i T_{ij,j} - \dot{\omega}_i (M_{ij,j} - e_{ikl} T_{kl}) - \dot{\psi}] dv, \tag{61}$$

then simplify and employ the equivalence (16): $\omega_i = -\frac{1}{2} e_{imn} \omega_{mn}$ between the rotation vector and skew-symmetric part of the displacement gradient tensor:

$$D = \int_D \left(T_{ij} v_{i,j} + M_{ij} \dot{\omega}_{i,j} - \frac{1}{2} e_{ikl} e_{imn} \dot{\omega}_{mn} T_{kl} - \dot{\psi} \right) dv, \tag{62}$$

to successively obtain:

$$D = \int_D (T_{ij} v_{i,j} + M_{ij} \dot{\omega}_{i,j} - \frac{1}{2} (\delta_{km}\delta_{ln} - \delta_{kn}\delta_{lm}) \dot{\omega}_{mn} T_{kl} - \dot{\psi}) dv \tag{63}$$

$$D = \int_D (T_{ij} v_{i,j} + M_{ij} \dot{\omega}_{i,j} - T_{ij} \dot{\omega}_{ij} - \dot{\psi}) dv, \tag{64}$$

$$D = \int_D (T_{ij} \dot{\epsilon}_{ij} + M_{ij} \dot{\omega}_{i,j} - \dot{\psi}) dv = \int_D (\mathbf{T} : \dot{\boldsymbol{\epsilon}} + \mathbf{M} : \mathbf{grad} \dot{\vec{\boldsymbol{\omega}}} - \dot{\psi}) dv. \tag{65}$$

Substituting Eq. (48) into Eq. (65), and using Eq. (28), it is seen that the dissipation is:

$$D = \int_D \left(T_{ij} \dot{\epsilon}_{ij}^p + M_{ij} \dot{\kappa}_{ij}^p \right) dv = \int_D \left(\mathbf{T} : \dot{\boldsymbol{\epsilon}}_p + \mathbf{M} : \dot{\boldsymbol{\kappa}}_p \right) dv \tag{66}$$

We now substitute in this relation the plastic curvature rate and strain rate obtained from the disclination and dislocation densities and velocities, as detailed in Eqs. (56), (58). In component form, we find:

$$D = \int_D \left(\frac{1}{2} T_{ij} \left(e_{jkl} \alpha_{ik} V_l^\alpha + e_{ikl} \alpha_{jk} V_l^\alpha \right) + M_{ij} e_{jkl} \theta_{ik} V_l^\theta \right) dv \tag{67}$$

or:

$$\begin{aligned} D &= \int_D \left(e_{jkl} \frac{T_{ij} + T_{ji}}{2} \alpha_{ik} V_l^\alpha + e_{jkl} M_{ij} \theta_{ik} V_l^\theta \right) dv \\ &= \int_D (\mathbf{F}_\alpha.\mathbf{V}_\alpha + \mathbf{F}_\theta.\mathbf{V}_\theta) dv, \end{aligned} \tag{68}$$

where $\mathbf{F}_\alpha$ and $\mathbf{F}_\theta$ are defined as:

$$\mathbf{F}_\alpha = \{\mathbf{T}\}.\boldsymbol{\alpha} : \mathbf{X}; F_l^\alpha = e_{jkl} \frac{T_{ij} + T_{ji}}{2} \alpha_{ik}, \tag{69}$$

$$\mathbf{F}_\theta = \mathbf{M}^t.\boldsymbol{\theta} : \mathbf{X}; F_l^\theta = e_{jkl} M_{ij} \theta_{ik}, \tag{70}$$

$\mathbf{F}_\alpha$ and $\mathbf{F}_\theta$ define the driving force for the dislocation and disclination velocity, respectively. When the disclinations are absent, the stress tensor is symmetric and the dissipation density is only due to dislocations (Acharya, 2003). Using the dyadic notation $\boldsymbol{\alpha} = \mathbf{b} \otimes \mathbf{t}$ for the dislocation density tensor per unit surface ($\mathbf{b}$ is a Burgers vector and $\mathbf{t}$ a line vector), the dislocation driving force (69) can also be written as: $\mathbf{F}_\alpha = \{\mathbf{T}\}.\mathbf{b} \times \mathbf{t}$, a form reminiscent of the Peach–Köhler force on discrete dislocations. This Peach–Köhler-type relationship still holds when couple-stresses are present, despite the non-symmetry of the stress tensor, which indicates that dislocation motion is insensitive to couple-stresses. If the disclination density tensor is also written in dyadic notation: $\boldsymbol{\theta} = \boldsymbol{\Omega} \otimes \mathbf{l}$ (again $\boldsymbol{\Omega}$ is a Frank's vector, $\mathbf{l}$ a line vector), the driving force associated with the disclination velocity is:

$$\mathbf{F}_\theta = \mathbf{M}^t.\boldsymbol{\Omega} \times \mathbf{l}, \tag{71}$$

a representation analog to the Peach–Köhler relationship for the driving force on dislocations. This driving force is normal to the disclination line, and is produced by the couple-stress tensor, with no contribution of the stress tensor. Positiveness of the dissipation rate (68) is ensured by choosing, in the simplest possible manner, constitutive relations in the form:

$$\mathbf{F}_\alpha = B_\alpha \mathbf{V}_\alpha; \quad B_\alpha > 0, \tag{72}$$

$$\mathbf{F}_\theta = B_\theta \mathbf{V}_\theta; \quad B_\theta > 0, \tag{73}$$

B_α and B_θ are positive material parameters, possibly varying with strain and curvature, the physical dimension of which is that of a stress divided by a length and a velocity. Eqs. (72) and (73) assume linear viscous drag and may be applicable at relatively high loading rate. They would need modification to account for thermally-activated motion of defects typical at low loading rates. Note that both the glide and non-glide components of the Peach–Köhler force are used to induce dislocation motion in Eq. (72), and that B_θ and the tensors of elastic constants ($\mathbf{A}$, $\mathbf{B}$, $\mathbf{D}$) are the only additional physical parameters requiring determination in the present model.

6. Solution algorithms

Gathering all the above governing equations, the model reads:

$$\mathbf{curl}\ \boldsymbol{\kappa}_p = -\boldsymbol{\theta}, \tag{74}$$

$$\mathbf{curl}\ \boldsymbol{\epsilon}_p = -\boldsymbol{\alpha} + \boldsymbol{\kappa}_p^t - tr(\boldsymbol{\kappa}_p)\mathbf{I}, \tag{75}$$

$$\mathbf{div}\ \mathbf{T} = 0, \tag{76}$$

$$\mathbf{div}\ \mathbf{M} + 2\vec{\mathbf{T}} = 0, \tag{77}$$

$$\dot{\boldsymbol{\kappa}}_p = \boldsymbol{\theta} \times \mathbf{V}_\theta, \tag{78}$$

$$\dot{\boldsymbol{\epsilon}}_p = \frac{1}{2}(\boldsymbol{\alpha}, \times \mathbf{V}_\alpha + (\boldsymbol{\alpha} \times \mathbf{V}_\alpha)^t), \tag{79}$$

$$\dot{\boldsymbol{\theta}} = -\mathbf{curl}\ \dot{\boldsymbol{\kappa}}_p, \tag{80}$$

$$\dot{\boldsymbol{\alpha}} = -\mathbf{curl}\ \dot{\boldsymbol{\epsilon}}_p + \dot{\boldsymbol{\kappa}}_p^t - tr(\dot{\boldsymbol{\kappa}}_p)\mathbf{I} = -\mathbf{curl}\ \dot{\boldsymbol{\epsilon}}_p + \mathbf{s}_\theta, \tag{81}$$

$$\mathbf{T} = \mathbf{C} : (\{\mathbf{gradu}\} - \boldsymbol{\epsilon}_p) + \mathbf{D} : (\mathbf{grad}\vec{\boldsymbol{\omega}} - \boldsymbol{\kappa}_p), \tag{82}$$

$$\mathbf{M} = \mathbf{A} : (\mathbf{grad}\vec{\boldsymbol{\omega}} - \boldsymbol{\kappa}_p) + \mathbf{B} : (\{\mathbf{gradu}\} - \boldsymbol{\epsilon}_p), \tag{83}$$

$$\mathbf{V}_\alpha = \frac{1}{B_\alpha}\{\mathbf{T}\}.\boldsymbol{\alpha} : \mathbf{X} \tag{84}$$

$$\mathbf{V}_\theta = \frac{1}{B_\theta}\mathbf{M}^t.\boldsymbol{\theta} : \mathbf{X}. \tag{85}$$

The unknowns are the dislocation and disclination tensors, and the displacement $\mathbf{u}$ and rotation vector $\vec{\boldsymbol{\omega}}$ fields. All the equations of field dislocation mechanics (Acharya, 2001), where the unknown variables are the dislocation tensor and displacement, generalize into pairs of equations. However, the solution algorithm is somewhat different, because dislocations are generated not only because the plastic strain has an incompatible part, but also through disclination mobility. Indeed, assuming that the disclination and dislocation densities are known at a step in time does provide the incompatible part of $\boldsymbol{\kappa}_p$ from Eq. (74) (using the side conditions mentioned in relation with Eq. (32)), but finding the incompatible part of $\boldsymbol{\epsilon}_p$ from Eq. (75) requires knowledge of the history-dependent compatible part of $\boldsymbol{\kappa}_p$. Therefore, the algorithm is as follows. Suppose an arbitrary distribution of dislocations and disclinations is known at the initial time and let the compatible part of the plastic curvature and plastic strain tensors arbitrarily set to zero, without loss of generality. Then, the incompatible parts of $\boldsymbol{\kappa}_p$ and $\boldsymbol{\epsilon}_p$ can be determined from Eqs. (74) and (75) respectively. Further, using the constitutive relations (82) and (83), the equilibrium problem (76) and (77) can be solved for the displacement and rotation vector fields, which are obtained uniquely, up to a rigid body motion. In addition, the plastic strain rate and curvature rate can be computed from Eqs. 78, 79, 84, 85, and utilized to update the plastic strain and curvature. In this algorithm, only the compatible parts of the plastic strain and curvature are needed for the update. Finally, the dislocation and disclination densities are updated using Eqs. (80) and (81), and the procedure can therefore be iterated at the next time step.

The rate form of the governing equations leads to a simpler incremental algorithm, to the expense of complete arbitrariness in the initial distribution of crystal defects. Taking the time derivative of Eqs. 76,77,82,83, the rate equations are:

$$\mathbf{div}\ \dot{\mathbf{T}} = 0, \tag{86}$$

$$\mathbf{div}\ \dot{\mathbf{M}} + 2\dot{\vec{\mathbf{T}}} = 0, \tag{87}$$

$$\dot{\boldsymbol{\kappa}}_p = \boldsymbol{\theta} \times \mathbf{V}_\theta, \tag{88}$$

$$\dot{\boldsymbol{\epsilon}}_p = \frac{1}{2}(\boldsymbol{\alpha} \times \mathbf{V}_\alpha + (\boldsymbol{\alpha} \times \mathbf{V}_\alpha)^t), \tag{89}$$

$$\dot{\boldsymbol{\theta}} = -\mathbf{curl}\ \dot{\boldsymbol{\kappa}}_p, \tag{90}$$

$$\dot{\boldsymbol{\alpha}} = -\mathbf{curl}\ \dot{\boldsymbol{\epsilon}}_p + \dot{\boldsymbol{\kappa}}_p^t - tr(\dot{\boldsymbol{\kappa}}_p)\mathbf{I} = -\mathbf{curl}\ \dot{\boldsymbol{\epsilon}}_p + \mathbf{s}_\theta, \tag{91}$$

$$\dot{\mathbf{T}} = \mathbf{C} : (\{\mathbf{gradv}\} - \dot{\boldsymbol{\epsilon}}_p) + \mathbf{D} : (\mathbf{grad}\dot{\vec{\boldsymbol{\omega}}} - \dot{\boldsymbol{\kappa}}_p), \tag{92}$$

$$\dot{\mathbf{M}} = \mathbf{A} : (\mathbf{grad}\dot{\vec{\boldsymbol{\omega}}} - \dot{\boldsymbol{\kappa}}_p) + \mathbf{B} : (\{\mathbf{gradv}\} - \dot{\boldsymbol{\epsilon}}_p), \tag{93}$$

$$\mathbf{V}_\alpha = \frac{1}{B_\alpha}\{\mathbf{T}\}.\boldsymbol{\alpha} : \mathbf{X}, \tag{94}$$

$$\mathbf{V}_\theta = \frac{1}{B_\theta}\mathbf{M}^t.\boldsymbol{\theta} : \mathbf{X}. \tag{95}$$

Suppose that all fields are known at a given step in time. The unknowns are the rotation rate $\dot{\vec{\boldsymbol{\omega}}}$ and material velocity $\mathbf{v}$ fields. They are solution to the rate of equilibrium problem 86,87,92, 93. In these equations, the plastic strain rate and curvature are obtained from the dislocation/disclination densities and stress/couple-stress tensors by using Eqs. (88) and (89) and (94) and (95). Once the dislocation and disclination densities are updated using Eqs. (90) and (91), the rate of equilibrium procedure can be iterated at the following time step. In this incremental scheme, the determination of the incompatible parts of the plastic curvature and strain arising from an initial distribution of crystal defects is avoided. Hence, in contrast with the first algorithm, there is no continuity requirement on the plastic curvature and strain, but only on their rates. Therefore, the solutions obtained from these two algorithms might turn out to be somewhat different. If the choice is made to also avoid the initial determination of the incompatible part of the plastic curvature and strain, then the relaxation of an arbitrarily chosen configuration of plastic strain and curvature may be used to define workable initial conditions, as will be shown below in Section 8. The numerical implementation couples a conventional Galerkin Finite Element scheme for the solution of the rate of equilibrium problem with a mixed Galerkin-Least Squares (GLS) Finite Element algorithm for the solution of the dislocation/disclination transport problem. Details of the latter can be found in Roy and Acharya (2005) and Varadhan et al. (2006). Exchanges of data between the two schemes are as follows. In the rate of equilibrium problem 86, 87, 92, 93, the plastic shear strain and curvature rates are inputs from the GLS scheme for dislocation/disclination transport. Conversely, the stress and couple-stress tensors, solutions to the equilibrium problem, are inputs for the GLS transport problem 88, 89.

7. A plane edge-wedge model

Let us consider a distribution of pure wedge disclinations. In an orthonormal reference frame $(\mathbf{e_1}, \mathbf{e_2}, \mathbf{e_3})$, let the disclination tensor be: $\boldsymbol{\theta} = \theta_{33}\mathbf{e_3} \otimes \mathbf{e_3}$, all other components being zero. In this simple setting, the continuity condition (33) implies: $\theta_{33,3} = 0$. Thus, the wedge disclination density θ_{33} only depends on the coordinates (x_1, x_2): $\theta = \theta(x_1, x_2)$. In component form, the rotational incompatibility Eq. (31) reads: $\theta_{ij} = -e_{jkl}\kappa^p_{il,k} = e_{jkl}\kappa^e_{il,k}$. In the present case, Eq. (31) reduces to:

$$\theta_{33} = \kappa^p_{31,2} - \kappa^p_{32,1} = \kappa^e_{32,1} - \kappa^e_{31,2}. \tag{96}$$

Hence the only relevant elastic and plastic curvatures are: $(\kappa^e_{31}, \kappa^e_{32})$ and $(\kappa^p_{31}, \kappa^p_{32})$. Additionally, we note that: $tr(\boldsymbol{\kappa}_p) = 0$. Thus, the disclination transport Eq. (55) is:

$$\dot{\theta}_{33} = \dot{\kappa}^p_{31,2} - \dot{\kappa}^p_{32,1}. \tag{97}$$

The plastic curvature rate (56) reads, in component form: $\dot{\kappa}^p_{ij} = e_{jkl}\theta_{ik}V^\theta_l$. Hence, we find:

$$\dot{\kappa}^p_{31} = -\theta_{33}V^\theta_2, \tag{98}$$

$$\dot{\kappa}^p_{32} = +\theta_{33}V^\theta_1. \tag{99}$$

Using the constitutive relation (73) for the disclination velocities provides their relationship with the couple-stresses:

$$V^\theta_1 = +\frac{1}{B_\theta}M_{32}\theta_{33}, \tag{100}$$

$$V^\theta_2 = -\frac{1}{B_\theta}M_{31}\theta_{33}. \tag{101}$$

Hence, the plastic curvature rates are:

$$\dot{\kappa}^p_{31} = \frac{1}{B_\theta} M_{31}\theta^2_{33}, \tag{102}$$

$$\dot{\kappa}^p_{32} = \frac{1}{B_\theta} M_{32}\theta^2_{33}, \tag{103}$$

and the disclination transport equation now reads:

$$\dot{\theta}_{33} = \frac{1}{B_\theta}\left(M_{31}\theta^2_{33}\right)_{,2} - \frac{1}{B_\theta}\left(M_{32}\theta^2_{33}\right)_{,1}. \tag{104}$$

Since the trace of the plastic curvature rate tensor is zero, the source term $\mathbf{s}_\theta$ in the dislocation transport Eq. (59) feeds only the edge dislocations densities $(\alpha_{13}, \alpha_{23})$. Using Eq. (58), it is seen that the motion of these dislocations produce the plastic strain rate components $(\dot{\epsilon}^p_{11}, \dot{\epsilon}^p_{12}, \dot{\epsilon}^p_{21}, \dot{\epsilon}^p_{22})$:

$$\dot{\epsilon}^p_{11} = -\alpha_{13} V^\alpha_2, \tag{105}$$

$$\dot{\epsilon}^p_{12} = \dot{\epsilon}^p_{21} = \frac{1}{2}\left(\alpha_{13} V^\alpha_1 - \alpha_{23} V^\alpha_2\right), \tag{106}$$

$$\dot{\epsilon}^p_{22} = +\alpha_{23} V^\alpha_1. \tag{107}$$

The relations (105) and (107) suggest that out-of-plane motion of the edge dislocations $(\alpha_{13}, \alpha_{23})$ is involved in the extension rates $(\dot{\epsilon}^p_{11}, \dot{\epsilon}^p_{22})$, whereas their glide is responsible for $\dot{\epsilon}^p_{12}$ in Eq. (106). Consistently, the dislocation transport Eq. (59) reduces to:

$$\dot{\alpha}_{13} = \dot{\epsilon}^p_{11,2} - \dot{\epsilon}^p_{12,1} + \dot{\kappa}^p_{31}, \tag{108}$$

$$\dot{\alpha}_{23} = \dot{\epsilon}^p_{21,2} - \dot{\epsilon}^p_{22,1} + \dot{\kappa}^p_{32}, \tag{109}$$

or, accounting for Eqs. (98), (99), (105)–(107):

$$\dot{\alpha}_{13} = -\left(\alpha_{13} V^\alpha_2\right)_{,2} - \frac{1}{2}\left(\alpha_{13} V^\alpha_1 - \alpha_{23} V^\alpha_2\right)_{,1} - \theta_{33} V^\theta_2 \tag{110}$$

$$\dot{\alpha}_{23} = -\left(\alpha_{23} V^\alpha_1\right)_{,1} + \frac{1}{2}\left(\alpha_{13} V^\alpha_1 - \alpha_{23} V^\alpha_2\right)_{,2} + \theta_{33} V^\theta_1. \tag{111}$$

Thus, if all other dislocation densities are initially absent, the dislocation distribution involves only α_{13} and α_{23} edge densities. The continuity Eq. (39) then implies that this distribution be a plane state: $\alpha_{13} = \alpha_{13}(x_1, x_2), \alpha_{23} = \alpha_{23}(x_1, x_2)$. The symmetric "Peach–Köhler" constitutive relation (72) provides the dislocation velocities in terms of the stress tensor, for both the out-of-plane motion of dislocations:

$$V^\alpha_1 = +\frac{1}{B_\alpha} T_{22}\alpha_{23} \tag{112}$$

$$V^\alpha_2 = -\frac{1}{B_\alpha} T_{11}\alpha_{13}, \tag{113}$$

and their glide:

$$V^\alpha_1 = +\frac{1}{2B_\alpha}(T_{12} + T_{21})\alpha_{13} \tag{114}$$

$$V^\alpha_2 = -\frac{1}{2B_\alpha}(T_{12} + T_{21})\alpha_{23}. \tag{115}$$

Therefore, the plastic strain rates induced by the motion of these dislocations are:

$$\dot{\epsilon}^p_{11} = \frac{1}{B_\alpha} T_{11}\alpha^2_{13} \tag{116}$$

$$\dot{\epsilon}^p_{12} = \dot{\epsilon}^p_{21} = \frac{1}{2B_\alpha}(T_{12} + T_{21})\left(\alpha^2_{13} + \alpha^2_{23}\right) \tag{117}$$

$$\dot{\epsilon}^p_{22} = \frac{1}{B_\alpha} T_{22}\alpha^2_{23}, \tag{118}$$

and the dislocation transport equation can be rewritten as:

$$\dot{\alpha}_{13} = +\frac{1}{B_\alpha}\left(T_{11}\alpha^2_{13}\right)_{,2} - \frac{1}{4B_\alpha}\left((T_{12} + T_{21})\left(\alpha^2_{13} + \alpha^2_{23}\right)\right)_{,1} + \frac{1}{B_\theta} M_{31}\theta^2_{33} \tag{119}$$

$$\dot{\alpha}_{23} = -\frac{1}{B_\alpha}\left(T_{22}\alpha^2_{23}\right)_{,1} + \frac{1}{4B_\alpha}\left((T_{12} + T_{21})\left(\alpha^2_{13} + \alpha^2_{23}\right)\right)_{,2} + \frac{1}{B_\theta} M_{32}\theta^2_{33}. \tag{120}$$

The stress and couple-stress components relevant to the present problem are $(T_{11},\ T_{12},\ T_{21},\ T_{22})$ and $(M_{31},\ M_{32})$ respectively. Hence the Cosserat balance of momentum Eqs. (45), (46) reduce to:

$$T_{11,1} + T_{12,2} = 0 \tag{121}$$

$$T_{21,1} + T_{22,2} = 0 \tag{122}$$

$$M_{31,1} + M_{32,2} + T_{21} - T_{12} = 0. \tag{123}$$

Thus, the loading applied at the boundaries of the body may include shear and tension/compression the directions $(\mathbf{e_1},\ \mathbf{e_2})$. Couple-stresses or rotations along the direction $\mathbf{e_3}$ may also be involved.

We now focus on describing the elastic properties in the model. In Eq. (41), the infinitesimal displacement $\boldsymbol{\kappa}_e \times \mathbf{r}.\mathbf{dr}$ arising from the curvatures $(\kappa^e_{31}, \kappa^e_{32})$ is zero at any point along any in-plane circuit C. Hence, the incompatible displacement due to the inhomogeneity of the lattice curvature is zero on any such circuit. Since these circuits allow characterizing all the dislocation densities present in the model, the contribution of the curvatures $(\kappa^e_{31}, \kappa^e_{32})$ to stresses is zero in Eq. (49). Hence we write:

$$T_{11} = C_{1111}\epsilon^e_{11} + C_{1122}\epsilon^e_{22} \tag{124}$$

$$T_{12} = C_{1212}\epsilon^e_{12} + C_{1221}\epsilon^e_{21} \tag{125}$$

$$T_{21} = C_{2112}\epsilon^e_{12} + C_{2121}\epsilon^e_{21} \tag{126}$$

$$T_{22} = C_{2211}\epsilon^e_{11} + C_{2222}\epsilon^e_{22}. \tag{127}$$

Assuming cubic symmetry of the crystal and denoting by μ the elastic shear modulus, the relations $C_{1111} = C_{2222} = \alpha\mu,\ C_{1122} = C_{2211} = \beta\mu,\ C_{1221} = C_{1212} = C_{2112} = C_{2121} = \gamma\mu$ hold, leaving only three independent non-dimensional constants: $(\alpha,\ \beta,\ \gamma)$ in relations (124), (127). In Eq. (50), the infinitesimal rotation $\mathbf{r} \times \boldsymbol{\epsilon}_e.\mathbf{dr}/r^2$ induced by the inhomogeneity of the in-plane strains $(\epsilon^e_{21}, \epsilon^e_{22})$ and $(\epsilon^e_{11}, \epsilon^e_{12})$ produce curvature components $(\kappa'_{31}, \kappa'_{32})$ respectively, giving rise in turn to couple-stress components $(M_{31},\ M_{32})$. We therefore conjecture the following relationship between the couple-stresses and the elastic curvatures and strains:

$$M_{31} = A_{3131}\kappa^e_{31} + B_{3121}\epsilon^e_{21} + B_{3122}\epsilon^e_{22} \tag{128}$$

$$M_{32} = A_{3232}\kappa^e_{32} + B_{3211}\epsilon^e_{11} + B_{3212}\epsilon^e_{12} \tag{129}$$

Assuming further $A_{3131} = A_{3232} = M\mu b^2$ and $B_{3211} = B_{3212} = -B_{3121} = -B_{3122} = \mu b$, where b the length of the Burgers vector and M a non-dimensional elastic modulus, we additionally conjecture that the characteristic length scale A_{3131}/B_{3112} involved by the elastic behavior is b. As already suggested, this internal length scale sets the characteristic dimension of the area over which inhomogeneity of the shear strains induces a significant couple stress component. Experimental measurements of the A_{ijkl} and B_{ijkl} elastic constants and of the viscosity constant B_θ have yet to be carried out. Provisionally, we adopt the values $M = 1$, consistent with an earlier estimate (Kröner, 1963), and a common value $B_\theta = B_\alpha = B$. The mobility of the disclinations might be overestimated by doing so, but this value conveniently allows showing the features of disclination dynamics in the following. Further, orders of magnitude found in Section 8 below seem to be consistent. The values of the parameters utilized in the forthcoming calculations are presented in Table 1. They are typical of aluminum. However, the non-dimensional elastic constants: (α, β, γ) are chosen in conformity with elastic isotropy: $\alpha = 2(1-\nu)/(1-2\nu), \beta = 2\nu/(1-2\nu), \gamma = 1$, with $\nu = 0.3$ for Poisson's ratio, in order to compare the elastic energy predicted in

Table 1
Numerical constants used in the model.

b	μ	b^2B	
0.27 nm	27 GPa	0.4×10^{-4} Pa s	
α	β	γ	M
3.5	1.5	1	1

the following for disclination dipoles with literature values (see below Eq. (130)).

Substituting $\left(\epsilon_{ij} - \epsilon^p_{ij}, \omega_{ij} - \kappa^p_{ij}\right)$ for $\left(\epsilon^e_{ij}, \kappa^e_{ij}\right)$ in the constitutive Eqs. (124)–(129), then the resulting stresses and couple-stresses in the balance of equilibrium Eqs. (121)–(123), one obtains three partial differential equations for the unknowns $(u_1,\ u_2,\ \omega_3)$. As already mentioned in Section 6, the plastic strain and curvature are updated by using the plastic strain and curvature rates (102), (103), (116)–(118), and the disclination and dislocation densities by using the transport Eqs. 104, 119, 120. Boundary conditions comprise the prescription of tractions and moments, or/and displacements and rotation on the surface of the body. Finally, the disclination and dislocation densities must be specified on inflow boundaries, but no condition is required on outflow boundaries.

8. Disclination dipoles

We consider a 75 nm × 75 nm square domain D in the crystal, and use a (15×15) finite element mesh of incomplete quadratic quadrangle elements to interpolate the unknown fields in the solution of the equilibrium problem, and of bilinear quadrangle elements in the transport problem. Integrations over all elements use a four Gauss points method. An arbitrary set of initial conditions is designed for the plastic curvatures $(\kappa^p_{31}, \kappa^p_{32})$ in order to position near the center of the body a nearly discrete dipole of wedge disclinations θ_{33}. As a first step in the determination of its dynamics, we let this tentative crystal defect re-arrange in its own stress and couple-stress fields, in accordance with the equilibrium and transport equations. In this process, the boundary ∂D of the domain D is kept free from applied stresses and couple-stresses. Any displacement and rotation is allowed on ∂D, and the lattice is left free to rotate. We shall refer to this process as the relaxation of the initial crystal defect, and monitor its evolution by plotting in time the total elastic free energy of the body. A well-defined and apparently stable defect pattern emerges from relaxation, as shown in Figs. 1 and 2. Initially enclosed in an arbitrary (5 nm × 5 nm) central square, the disclination and dislocation densities quickly spread out and stabilize within a much larger circular area, about 60 nm in diameter, as seen in Fig. 1. In this figure, the disclination density is color-coded, and the dislocation densities can be apprehended through the field of Burgers vectors. At each point in this area, the disclination and dislocation densities combine to produce a complex crystal defect. However, we believe that this pattern would slowly and steadily expand if an infinitely long computation time was allowed for its complete relaxation. Such expansion would occur in relation with the linearity of the elastic constitutive relations (49) and (50). We conjecture a definitely (meta) stable confinement of the defect within the body could be realized if a non convex elastic potential was utilized. Employing Eq. (42), the Frank's vector magnitude over the half positive, D_1, and half negative, D_2, parts of the resulting dipole is obtained as: $\Omega = \int_{D_1} \theta_{33} dS = -\int_{D_2} \theta_{33} dS = 0.3 rad$. Using Eq. (43), the total Burgers vector of the dipole is found as: $\mathbf{b} = \frac{\sqrt{2}}{2} b(-\mathbf{e_1} + \mathbf{e_2})$; $b = 15$ nm. Through the intimate connections between the rotation gradient and Burgers vector fields evidenced in Fig. 2, the intertwinning of the dislocation and disclination fields is self-obvious.

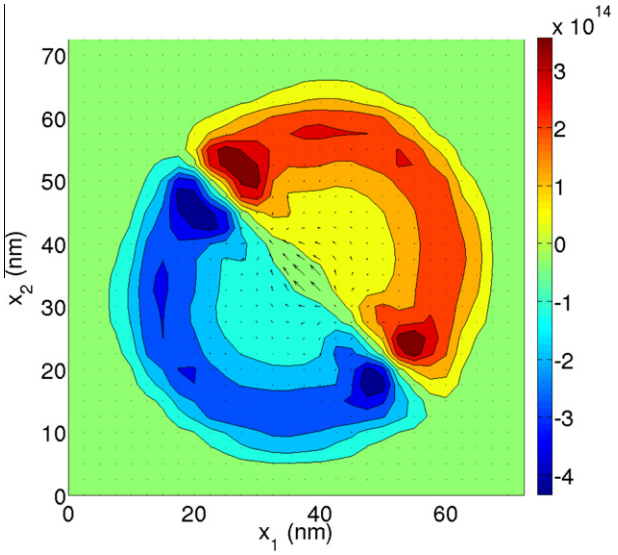

Fig. 1. Disclination density θ_{33} and Burgers vector fields in domain D after relaxation. The disclination density is color-coded in m^{-2} units. The arrows represent the local Burgers vector, whose components are the edge dislocation densities $(\alpha_{13},\ \alpha_{23})$ per unit surface. The dislocation and disclination lines are along the normal to the figure.

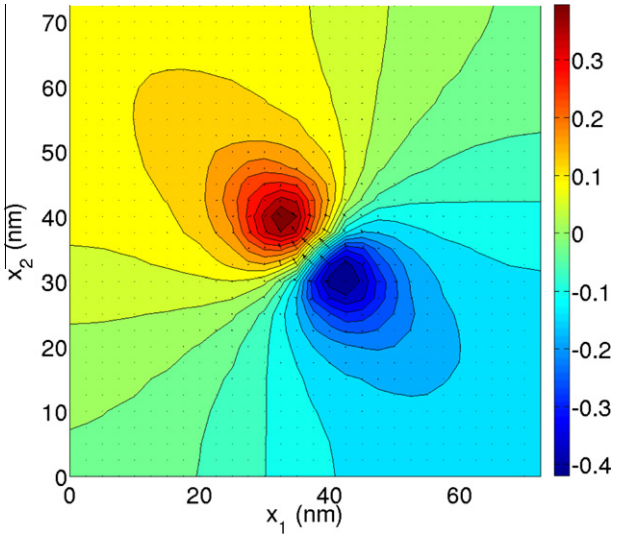

Fig. 2. Rotation ω_3 and Burgers vector field in domain D after relaxation. The dislocation lines and rotation axis sit along the normal to the figure. The rotation is color-coded in radians. The arrows represent the local Burgers vector, whose components are the edge dislocation densities $(\alpha_{13},\ \alpha_{23})$ per unit surface (also shown in Fig. 1). In areas where the incompatibility is small, the Burgers vector is approximately aligned with the gradient vector of ω_3.

Indeed, subtracting Eq. (35) from Eq. (34), it can be shown that: $\mathbf{grad}\vec{\omega} \approx 2\boldsymbol{\alpha}^t$, or: $\omega_{3,j} \approx 2b_j; j = 1, 2$, in the regions where incompatibility is small before the compatible plastic curvature. Hence, the gradient vector of ω_3 is approximately aligned with the Burgers vector in areas where relaxation dislocations nucleated by transport of disclination densities are prevailing. From Fig. 3, it is seen that the elastic free energy converges in less than a μs to the final value: $\psi = 2 \times 10^{-9}$ J/m, much smaller than the initial value: $\psi = 5.5 \times 10^{-9}$ J/m. It is worth comparing this result with the elastic energy E_Ω of a two-axes discrete disclination dipole, as provided by the linear isotropic elasto-static theory of disclinations (Romanov and Vladimirov, 1992; Romanov and Kolesnikova, 2009):

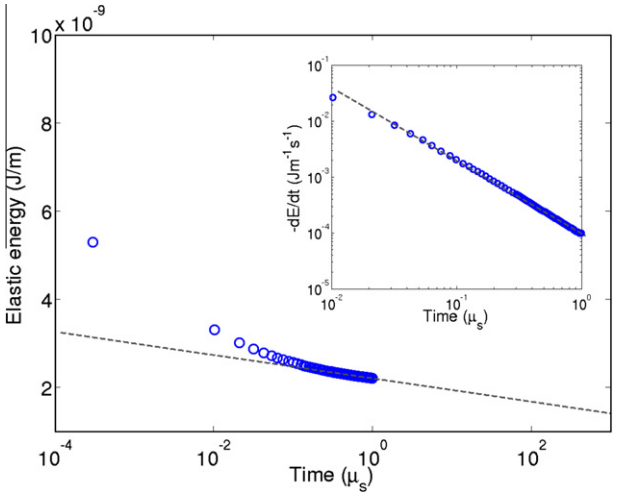

Fig. 3. Elastic energy of the crystal defect during relaxation in semi-logarithmic coordinates. The dotted lines are a guide to the eye. The insert displays the time derivative of the elastic energy in logarithmic coordinates, showing power-law dependence with exponent close to 1.

$$E_\Omega = \frac{\mu}{2\pi(1-\nu)}\Omega^2 a^2 (2\ln\frac{R_s}{2a} + 3). \tag{130}$$

Here $2a$ is the dipole arm, i.e., the separation distance between the disclination axes in Fig. 1 ($2a = 5$ nm), and R_s is a screening distance (here: 75 nm, the size of the body). Hence, we find: $E_\Omega \approx 3\times 10^{-8}$ J/m, a value 15 times larger than the energy of the relaxed crystal defect. To sum up, it seems that in the course of relaxation, through transport driven by their self-couple-stress field, discrete disclination dipoles evolve into well-defined crystal defects extended in space and involving relaxation dislocations, in a way such that their elastic free energy reaches much smaller levels than believed on the basis of elasto-static calculations. Interestingly, the time dependence of the elastic energy during relaxation is close to logarithmic (see Fig. 3). The relaxed configuration of an initial "discrete" disclination dipole with a wide separation distance $2a = 60$ nm along the $\mathbf{e_1}$ direction is shown in Fig. 4 and the corresponding rotation field in Fig. 5. In the relaxation process, transport of the wedge dipole under its own stress and couple-stress field generates a linear array of α_{23} edge dislocations forming a tilt segment enclosed in the dipole. The rotation field exhibits a continuous shift across the tilt segment, to produce a 36° misorientation in less than 10 nm. Hence, the dipole may be considered as modeling a high-angle tilt boundary segment with a finite width. More elaborate modeling of grain boundaries, using the relaxation of arrays of disclination dipoles as introduced in (Gertsman et al., 1989) will be envisioned in future work.

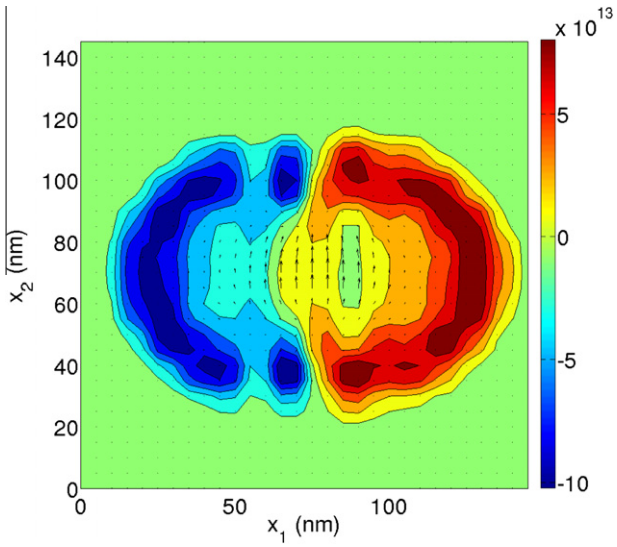

Fig. 4. Disclination dipole with separation distance $2a = 60$ nm. Disclination density θ_{33} and Burgers vector fields in domain D after relaxation. The disclination density is color-coded in m^{-2} units. The arrows represent the local Burgers vector, whose components are the edge dislocation densities (α_{13}, α_{23}) per unit surface. The dislocation and disclination lines are along the normal to the figure.

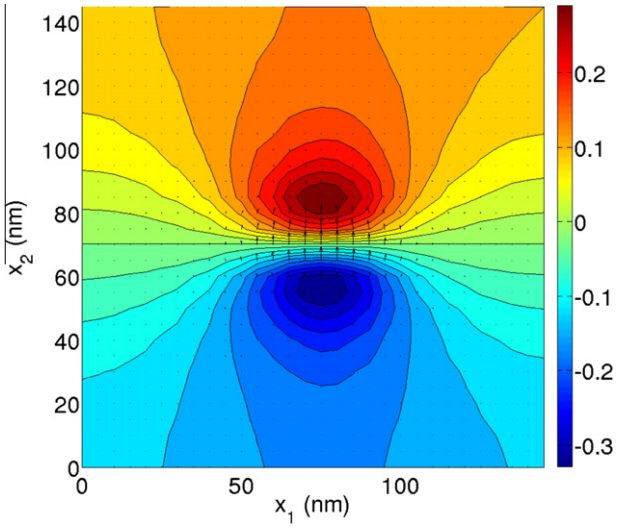

Fig. 5. Disclination dipole with separation distance $2a = 60$ nm. Rotation ω_3 and Burgers vector field in domain D after relaxation. The dislocation lines and rotation axis sit along the normal to the figure. The rotation is color-coded in radiants. The arrows represent the Burgers vector field, also shown in Fig. 4.

We now consider relaxing a point-disclination dipole to its stable self-organized configuration, and sequentially performing transverse tensile loading along the "vertical" $\mathbf{e_2}$ axis, normal to the dipole direction $\mathbf{e_1}$. During the loading sequence, the displacement of the body is set to zero at one point on the lower boundary, while the rest of the boundary has no vertical displacement but is free to move in the "horizontal" $\mathbf{e_1}$ direction. On the upper boundary, the vertical displacement is prescribed at a constant positive velocity, such that the applied strain rate is $\dot{\epsilon}^a_{22} = 10^4$ s^{-1}, while the horizontal component of the displacement is also free. In addition, the rotation is free on all boundaries. The relaxed configuration is shown in Fig. 6, inset A1. The disclination density and Burgers vectors shown are similar to those in Fig. 4. The corresponding α_{23} edge-density is additionally shown in the inset A2.[2] The rotation misfit across the dipole is 36°. The figures B1 and B2 are evolved from A1 and A2 after about 7% total tensile strain in the loading sequence. It is seen that the disclination dipole stretches and moves in both directions. The positive disclination stretches in the direction normal to the dipole, while slightly moving to the right in the dipole direction. The negative disclination shrinks toward the dipole axis, while being essentially motionless. In the mean time, the α_{23} edge dislocations are transported to the right along the dipole by out-of-plane motion, possibly by climb or atom shuffling (see the Burgers vectors evolutions in the main figure), which induces a significant plastic strain (about 2%) when the traction reaches its max-

[2] To improve the numerical stability of the solutions to the transport Eqs. 104, 119, 120 in tensile loading, the numerical diffusion parameter was set to a slightly higher value than in a simple relaxation process (see details on the algorithm in Varadhan et al. (c2006)). As a result, the relaxed α_{23} edge dislocation density is more evenly distributed in the dipole. We checked that such a slight discrepancy has no influence on the results shown in Fig. 6.

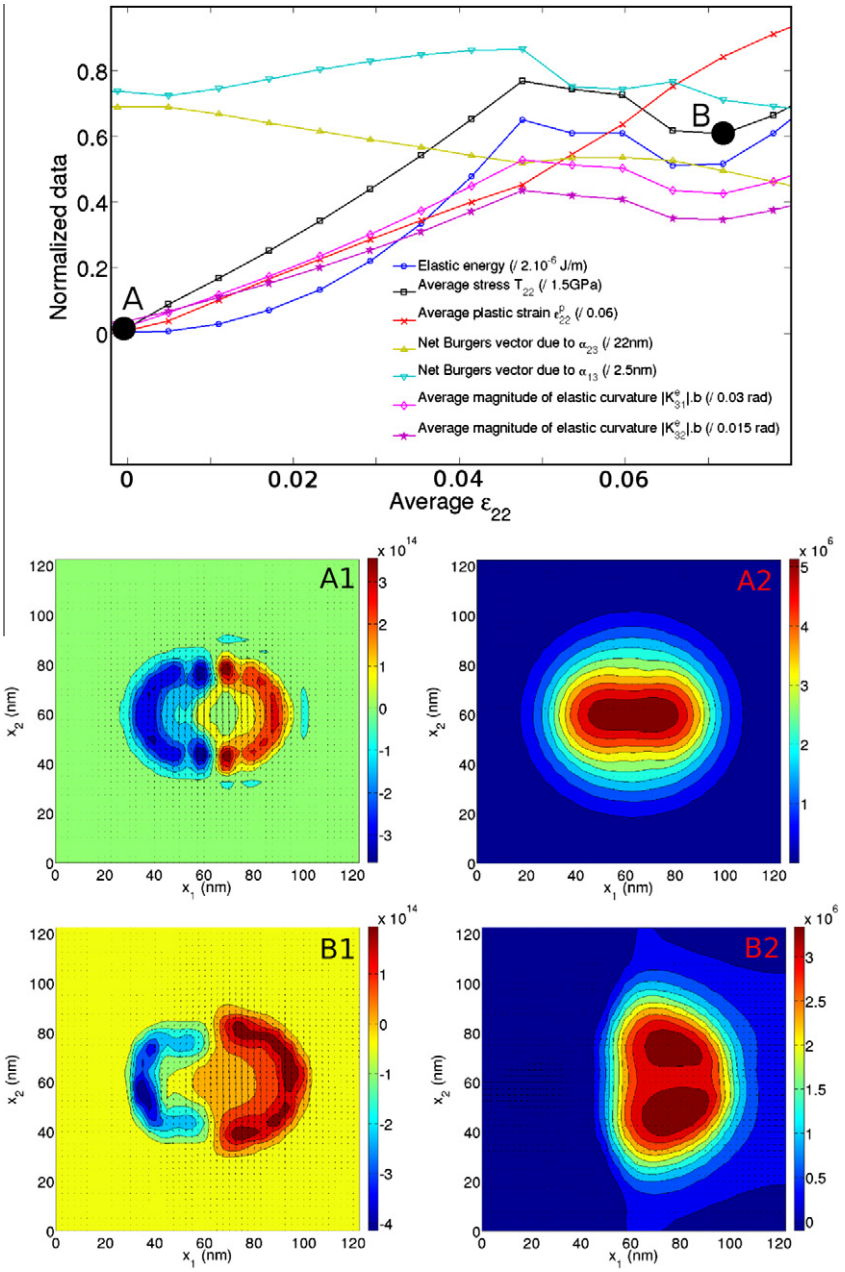

Fig. 6. Tensile loading of a relaxed disclination dipole with separation distance $2a = 30$ nm. Subset A includes color-coded maps of the relaxed disclination density and Burgers vector distribution (represented by arrows) (A1), edge-dislocation density α_{23} and the corresponding velocity (arrows) (A2). Subset B shows the figures evolved from A1 and A2 after approximately 7% total strain. The main figure includes normalized plots of the elastic energy of the body (blue line, circles, marks corresponding to subsets A and B), tensile stress (black line, squares), tensile plastic strain (red line, crosses), Burgers vector magnitude of the α_{23} edge-dislocations (up triangles), Burgers vector magnitude of the α_{13} edge-dislocations (down triangles), average magnitude of elastic curvature κ^e_{31} (diamonds) and average magnitude of elastic curvature κ^e_{32} (stars). The applied strain rate is $\dot{\epsilon}^a_{22} = 10^4\ s^{-1}$.

imum value $T_{22} = 1.1$ GPa. In the process, the elastic curvatures $(\kappa^e_{31}, \kappa^e_{32})$ and the total rotation gap between the upper and lower sides of the dipole increase. Recall that the rotation is free at the boundaries, a condition not likely to be realistic if the simulation box is seen as part of a bicrystal, but useful here to demonstrate rotation of the crystallites, a prominent feature of the deformation process. Nucleation of $(\alpha_{13}, \alpha_{23})$ edges occurs when the tensile stress and elastic energy of the body decrease at yield. Eventually, the tensile plastic strain reaches 6%, due to the out-of-plane motion of the α_{23} edges to the right of the dipole (see the Burgers vectors evolution in Fig. 6, and inset B2 where the arrows show the velocity of the α_{23} edges). Note that, because the displacement of the body is unconstrained in the dipole direction, the transverse strain ϵ_{11} is everywhere of the order of 10^{-3} during the loading process, and that the increase in the elastic energy of the body is essentially due to the elastic tensile strain and curvatures.

Comparison of these predictions with experimental data and results from atomistic simulations is desirable. Recent experimental work showed that nanocrystalline aluminum, with average grain size 60 nm, dynamically compressed at a strain rate of 2636 s^{-1} using a Split Hopkinson Pressure Bar, yields at 800 Mpa (Khan et al., 2006). Such a high yield stress level results from both the small grain size and the high applied strain rate. Hence, although the experimental conditions are rather different (loading path, sample size, applied strain rate and boundary conditions), the positive rate sensitivity of the yield stress suggests that the 1.1 GPa

value obtained in transverse tension at a strain rate of $10^4\ s^{-1}$ could be plausible. Further, some aspects of the tilt boundary behavior under transverse uniaxial tensile and compressive loading in copper were recently investigated using atomistic simulations (Tschopp et al., 2008; Spearot et al., 2008). The yield stress obtained from the simulations (Tschopp et al., 2008) has values significantly larger than ours, of the order of $3.1 - 3.4$ GPa, perhaps due to more constrained boundary conditions and a much larger strain rate level. In these simulations however, dislocation nucleation is not seen before the tensile stress reaches its maximum, at which point the simulations are stopped. In the present work, edge dislocation nucleation and plastic straining occur earlier during the loading sequence. It is also of interest to note that, under tension normal to the dipole direction, with boundary conditions such that the elastic strain in the direction of the dipole remains negligible, the elastic energy of the body sharply increases until plastic relaxation occurs, consistent with ideas conveyed in (Spearot et al., 2008).

9. Conclusions

A linearized theory of the elasto-plasticity of crystalline materials accounting for both translational and rotational crystal defects, i.e., dislocations and disclinations, was proposed. The most original contributions of this work can be summarized as follows: (i) It was shown how, in particular by using the transport equations for dislocations and disclinations as evolution equations, the elasto-static theory of disclination fields (deWit, 1970) can be extended to become an elasto-plastic dynamic theory, (ii) The elasto-plastic theory of dislocation fields (Acharya, 2001) was extended and regularized in the sense that the proposed theory is able to deal with discontinuities of the elastic rotation field, (iii) On thermodynamical grounds, it was demonstrated that the mobility of disclinations is driven by the couple-stress tensor and that of dislocations by the stress tensor exclusively. The ensuing Peach–Köhler-type driving forces for dislocations and disclinations were defined, and dissipative constitutive relations were proposed. As a proof of concept and in order to show the applicability of the theory, a simple plane edge-wedge model was developed. The relaxation of a point-disclination dipole into a self-organized dislocation–disclination pattern, and its behavior under tensile loading normal to its axis were detailed. The results suggest that the model may be used for further grain-boundary modeling and study of grain boundary-mediated plasticity. This will be an objective of future work.

The size of the bodies to be investigated by using the present approach can be of the order of (but may be larger than) the dimensions of the atomistic samples studied in molecular dynamics simulations. We emphasize that using a continuous approach at length scales below the elementary lattice parameters is still fully meaningful. As K. Kondo puts it: "No lower limit is...categorically imposed on the terminology of differential geometry of continua. Hence all the microscopic complications in scales much lower than the lattice and dislocation structures could tacitly be included in the formula" (Kondo, 1964). Besides, the time scale of our computations is much larger than that of molecular dynamics simulations. In the present work, the simulations were carried out on a single-processor desktop computer, which leaves room for substantial improvement in computational performance. Nevertheless the loading strain rate was 10^5 smaller than the typical strain rates employed in standard atomistic simulations. Diffusion related phenomena such as climb of dislocations, which can hardly be envisioned in the latter due to the exceedingly high loading rates that are employed, can be dealt with in the present approach. This feature may be of interest in the study of grain-boundary mediated plasticity, where diffusion-related phenomena could play a role (Mompiou et al., 2009).

References

Acharya, A., 2001. A model of crystal plasticity based on the theory of continuously distributed dislocations. J. Mech. Phys. Solids 49, 761.

Acharya, A., 2003. Driving forces and boundary conditions in continuum dislocation mechanics. Proc. Roy. Soc. Lond. A459, 1343–1363.

Bilby, B.A., 1955. Types of dislocation source. In: Bristol Conference Report on Defects in Crystalline Solids, The Physical Society, London, p. 124.

Coleman, B.D., Gurtin, M.E., 1967. Thermodynamics with internal state variables. J. Chem. Phys. 47, 597–613.

Cosserat, E., Cosserat, F., 1909. Théorie des Corps déformables. Hermann, Paris.

deWit, R., 1970. Linear theory of static disclinations. In: Fundamental aspects of dislocation theory. In: Simmons, J.A., de Wit, R., Bullough, R. (Eds.), NBS Spec. Publ. 317, vol. 1, pp. 651–680 (National Bureau of Standards, Washington, DC).

Frank, F.C., 1950. The resultant content of dislocations in an arbitrary intercrystalline boundary, In: Symposium on The Plastic Deformation of Crystalline Solids, Mellon Institute, Pittsburgh, (NAVEXOS-P-834), p. 150.

Friedel, J., 1964. Dislocations. Pergamon, London.

Gertsman, V. Yu., Nazarov, A.A., Romanov, A.E., Valiev, R.Z., Vladimirov, V.I., 1989. Disclination-structural unit model of grain boundaries. Phil. Mag. A 59, 1113.

Hurtado, J.A., Eliott, B.R., Shodja, H.M., Gorelikov, D.V., Campbell, C.E., Lippard, H.E., Isabell, T.C., Weertmann, J., 1995. Disclination grain boundary model with plastic deformation by dislocations. Mat. Sci. Eng. A190, 1.

Khan, A.K., Suh, Y.S., Chen, X., Takacs, L., Zhang, H., 2006. Nanocrystalline aluminum and iron: mechanical behavior at quasi-static and high strain rates, and constitutive modeling. Int. J. Plast. 22, 195209.

Kleman, M., Friedel, J., 2008. Disclinations, dislocations, and continuous defects: a reappraisal. Rev. Mod. Phys. 80, 61.

Kondo, K., 1964. On the analytical and physical foundations of the theory of dislocations and yielding by the differential geometry of continua. Int. J. Eng. Sci. 2, 219–251.

Kossecka, E., deWit, R., 1977. Disclination kinematics. Arch. Mech. 29, 633–651.

Kossecka, E., deWit, R., 1977. Disclination dynamics. Arch. Mech. 29, 749–767.

Kröner, E., 1958. Kontinuumstheorie der Verstetzungen and Eigenspannungen. In: Collatz, L., Lösch, F. (Eds.), Ergebnisse der Angewewandte Mathematik, vol. 5. Springer, Heidelberg, pp. 1–179.

Kröner, E., 1963. On the physical reality of torque stresses in continuum mechanics. Int. J. Eng. Sci. 1, 261–278.

Kröner, E., 1980. Continuum theory of defects. In: Balian, R. et al. (Eds.), Physics of Defects. North Holland, Amsterdam, pp. 218–314.

Li, J.C.M., 1972. Disclination model of high angle grain boundaries. Surface Sci. 31, 12.

Mompiou, F., Caillard, D., Legros, M., 2009. Grain boundary shear-migration coupling – I. In situ TEM straining experiments in Al polycrystals. Acta Mater. 57, 2198–2209.

Mura, T., 1963. Continuous distributions of moving dislocations. Phil. Mag. 89, 843.

Nye, J.F., 1953. Some geometrical relations in dislocated crystals. Acta Metall. 1, 153.

Romanov, A.E., Vladimirov, V.I., 1992. Disclinations in crystalline solids. In: Nabarro, F.R.N. (Ed.), Dislocations in Solids, vol. 9. Elsevier, Amsterdam, p. 191.

Romanov, A.E., Kolesnikova, A.L., 2009. Application of disclination concept to solid structures. Prog. Mat. Sci. 54, 740.

Roy, A., Acharya, A., 2005. Finite element approximation of field dislocation mechanics. J. Mech. Phys. Solids 53, 143.

Shih, K.K., Li, J.C.M., 1975. Energy of grain boundaries between cusp misorientations. Surface Sci. 50, 109.

Spearot, D.E., Capolungo, L., Qu, J., Cherkaoui, M., 2008. On the elastic tensile deformation of $< 100 >$ bicrystal interfaces in copper. Comput. Mater. Sci. 42, 57–67.

Sutton, A.P., Vitek, V., 1983. On the structure of tilt grain boundaries in cubic metals. I. Symmetrical tilt boundaries. Phil. Trans. Roy. Soc. London A309, 1.

Tschopp, M.A., Tucker, G.J., McDowell, D.L., 2008. Atomistic simulations of tension–compression asymmetry in dislocation nucleation for copper grain boundaries. Comput. Mater. Sci. 44, 351–362.

Upadhyay, M., Capolungo, L., Taupin, V., Fressengeas, C., in press. Grain boundary and Triple line energies in crystalline media: a disclination based approach. Int. J. Solids Structures. doi:10.1016/j.ijsolstr.2011.07.009.

Varadhan, S., Beaudoin, A.J., Acharya, A., Fressengeas, C., 2006. Dislocation transport using an explicit Galerkin/least-squares formulation. Modelling Simul. Mater. Sci. Eng. 14, 1.

Volterra, V., 1907. Sur l'équilibre des corps élastiques multiplement connexes. Ann. Sci. Ecol. Norm. Sup. III 24, 401–517.

Weingarten, J., 1901. Atti. Accad. Naz. Lincei. Cl. Sci. Fis. Mat. Natur. Rend. 10 (1), 57.